Statistics of Envelope of High-Frequency Ultrasonic Backscatter from Human Skin In Vivo

Balasundar I. Raju and Mandayam A. Srinivasan

Abstract—**The statistics of envelope of high-frequency ultrasonic backscatter signals from in vivo normal human dermis and subcutaneous fat were studied. The capability of six probability distributions (Rayleigh, Rician, K, Nakagami, Weibull, and Generalized Gamma) to model empirical envelope data was studied using the Kolmogorov-Smirnov (KS) goodness of fit statistic. The parameters of all the distributions were obtained using the maximum likelihood method. It was found that the Generalized Gamma distribution with two shape parameters provided the best fit among all the distributions in terms of the KS goodness of fit. The K and Weibull distributions also modeled the envelope statistics well. The Rayleigh and Rician distributions provided poorer fits. The parameters of the Generalized Gamma distribution, however, showed a larger variability than those of the other distributions. The intersubject variability in the estimated parameters of all the distributions was found to be comparable to the intrasubject variability. Fat was seen to exhibit significantly more pre-Rayleigh behavior compared to the dermis. The parameters of the Generalized Gamma distribution also showed significant differences between the dermis at the forearm and fingertip regions.**

I. Introduction

High frequency ($\geq$ 20 MHz) ultrasound has several applications in dermatology, such as the evaluation of tumors, scleroderma, psoriasis, contact dermatitis, burn injuries, and sun damage. However, conventional B-scan images of the skin do not fully exploit the information contained in the backscattered echoes, and quantitative tissue characterization studies might provide additional information about these tissues. The need for such studies is evident from earlier works which have shown that, when using B-scan images of the skin, it is often difficult to distinguish between benign and malignant lesions [1], between different types of skin tumors [1], [2], between melanoma and a scar tissue [3], or between tumors and subtumoral inflammatory infiltrate [4]. It is conceivable that, given the vast variety of skin ailments, quantitative methods might provide additional information for classifying various skin tissues.

Manuscript received December 11, 2001; accepted March 4, 2002. The work reported here was partly funded by NIH-NINDS grant NS33778 and by a Grant-in-Aid of research from the National Academy of Sciences through Sigma Xi.

The authors are with the Laboratory for Human and Machine Haptics, Research Laboratory of Electronics, Massachusetts Institute of Technology, Cambridge, MA (e-mail: raju@mit.edu).

One approach for obtaining additional information for characterizing tissues using ultrasound is analyzing the statistical fluctuations of the backscattered signals. Ultrasonic signals can be modeled as stochastic signals, because the precise details of the scattering structures in tissues, and consequently the details of the backscattered signals, are not known a priori. In prior studies, the first order statistics of the amplitude of backscattered signals from several tissues—such as the liver [5], [6], heart [7]–[9], breast [10], eye [11], and kidney [12]—have been studied. Parameters related to amplitude statistics—such as the scatterer number density [12], [13] and its frequency dependence [14]—also have been studied for their potential for tissue characterization. Moreover, second order statistics also have been studied [15]. Much of the theoretical background for such studies was obtained from earlier works in other fields, such as optics, radar, and communications.

To realize the goal of better discrimination of skin tissues with ultrasound, in this paper we study the first order statistics of envelope of backscattered signals from normal human dermis and subcutaneous fat. The reasons for the present study and its contributions are as follows. Until now, tissue characterization studies of skin have been sparse, and very little information on ultrasound-skin interaction is available. Previous studies in this regard have involved only attenuation [16]–[20] and backscatter [16], [20] coefficients of skin tissues. Until now, the statistical distributions of the envelope of backscattered signals from skin tissues have not been studied. The type of probability distribution of the envelope signals, and their parameters, could contain potential information regarding tissue microstructure that could be exploited for tissue characterization. In this work, we study the capability of six different probability distributions (Rayleigh, Rician, K, Nakagami, Weibull, and Generalized Gamma) to model the statistics of envelope of backscattered data collected from the skin of several human volunteers in vivo using the Kolmogorov-Smirnov (KS) statistic as a goodness of fit measure. We also study the variability in parameter estimates and compare inter- and intrasubject variability. This is important as a large variability in the estimates might limit the capability of the parameters for tissue characterization and methods to reduce such variability should be pursued. The capability of the parameters to differentiate different skin tissues (dermis vs. fat, forearm dermis vs. fingertip dermis) is also studied.

II. Probability Density Functions

The signal received by an ultrasound transducer can be modeled as a phasor sum of the returns from several scatterers within the resolution cell of the system:

$$re^{j\psi} = \sum_{i=1}^{n} a_i e^{j\theta_i}, \tag{1}$$

where a_i's are the amplitudes of signals scattered from the individual scatterers, which in turn depend on the shape, size, and acoustical properties of the scatterers and the surrounding medium, and the θ_i's depend on the position of the scatterers. Because the precise details regarding the scattering cross sections of the individual scatterers are unknown, the a_i's are modeled as random variables. Also, because the locations of the scatterers are unknown, the θ_i's are also modeled as random variables. Moreover, n, the number of scatterers contributing to the resultant, also can be a random quantity in general. Hence, the resultant amplitude r is also a random quantity that can be described using probability density functions (pdfs). It should be pointed out that the model presented in (1) is an idealized one because realistic scattering occurs continuously throughout the tissue and not at discrete points. Nevertheless, it provides a convenient starting point for analysis. Even with this simplified model, it generally is difficult to obtain the exact pdf of the amplitude r, except when n is small and the θ_i's are assumed to be uniformly distributed between 0 and 2π [21]. In practice, several well-known distributions are used to describe the pdf of r, and their appropriateness is evaluated using goodness of fit measures. In making such a description, one desires that the distribution fits empirical data well and is sufficiently rich enough to model a variety of scattering conditions. With the aim of determining the pdf that best models backscatter data from skin tissues, six probability distributions summarized below were studied in this work. Expressions for their pdfs, denoted as $p(r)$, and their cumulative distribution functions (cdfs), denoted as $F(r)$, also are given. The expressions for the cdfs were used in computing the KS goodness of fit measures. Also mentioned are the bounds on the ratio of the mean to standard deviation, denoted as SNR.

A. Rayleigh Distribution

The Rayleigh distribution [22] results as a consequence of the central limit theorem, when the scattering medium contains a large number of randomly distributed scatterers (θ_i's uniformly distributed between 0 and 2π). It also can result if the individual scattering amplitudes a_i in (1) are themselves Rayleigh distributed, even for finite n. Its pdf and cdf are given by:

$$p(r) = \frac{r}{\sigma^2} e^{-\left(\frac{r^2}{2\sigma^2}\right)} \qquad r \geq 0;\ \sigma > 0 \tag{2}$$

$$F(r) = 1 - e^{-\left(\frac{r^2}{2\sigma^2}\right)} \tag{3}$$

For this distribution, the SNR is equal to 1.91.

B. Rician Distribution

The Rician distribution [23] results if, in addition to conditions leading to the Rayleigh distribution, a specular or unresolved coherent component exists yielding the following pdf and cdf for the amplitude of the resultant phasor:

$$p(r) = \frac{r}{\sigma^2} e^{-\left(\frac{r^2+s^2}{2\sigma^2}\right)} I_0\left(\frac{sr}{\sigma^2}\right) \qquad r \geq 0;\ s \geq 0,\ \sigma > 0 \tag{4}$$

$$F(r) = 1 - Q_1\left(\frac{s}{\sigma}, \frac{r}{\sigma}\right), \tag{5}$$

where $I_0(x)$ is the modified Bessel function of the first kind of order 0, Q_1 is the Marcum Q function [24], and s is the amplitude of the coherent term. The Rician distribution includes the Rayleigh distribution as a special case for $s = 0$. The SNR for this distribution is ≥ 1.91.

C. K Distribution

The K distribution [25] results when the θ_i's are distributed uniformly between 0 and 2π, and the number of scatterers is random and follows negative binomial statistics, provided the mean number of scatterers is large. This distribution also arises if the individual scattering amplitudes a_i's are themselves K distributed, even for finite n. The pdf and cdf are given by:

$$p(r) = 2\left(\frac{r}{2}\right)^{\alpha} \frac{b^{\alpha+1}}{\Gamma(\alpha)} K_{\alpha-1}(br) \qquad r \geq 0;\ \alpha, b > 0 \tag{6}$$

$$F(r) = 1 - \frac{2}{\Gamma(\alpha)} \left(\frac{br}{2}\right)^{\alpha} K_{\alpha}(br), \tag{7}$$

where α and b are the shape and scale parameters, respectively, and $K_\alpha(x)$ is the modified Bessel function of the second kind of order α. The relationship between the Rayleigh and K distributions was given by Jakeman and Tough [26], who showed that a Rayleigh process with nonconstant second-moments is K distributed. Thus, variations in scattering cross sections of the individual scatterers tend to lead to deviations from the Rayleigh distribution to the K distribution. The K distribution includes the Rayleigh distribution as a special case for $\alpha = \infty$, and has an SNR ≤ 1.91.

D. Nakagami Distribution

The Nakagami distribution, first derived by Nakagami [27] based on his large-scale observations in high-frequency, long-distance radio propagation, has the following expressions for the pdf and cdf:

$$p(r) = \frac{2m^m}{\Gamma(m)\Omega^m} r^{(2m-1)} e^{-\left(\frac{mr^2}{\Omega}\right)} \qquad r \geq 0;\ m, \Omega > 0 \tag{8}$$

$$F(r) = \Gamma_{\text{inc}}\left(m, \frac{mr^2}{\Omega}\right), \tag{9}$$

where m and Ω are the shape and scale parameters, respectively, and $\Gamma_{\text{inc}}(m, x)$ is the incomplete gamma function. Although derived empirically, theoretical justifications for encountering this type of distribution were provided by Yacoub [28] based on the observation that the power of a Nakagami distributed signal is the same as that of another signal composed of the incoherent sum of several Rayleigh signals. For example, if signals from two Rayleigh regions are added coherently, the sum has a Rayleigh envelope. However, if these signals are added incoherently (powers added rather than instantaneous amplitudes), the resultant power is the sum of two exponential random variables, which is gamma distributed, in which case the amplitude is Nakagami distributed. Thus, the Nakagami signal can be understood to be composed of clusters of waves added incoherently, for which within any one cluster the resultant obeys Rayleigh statistics, and the clusters are randomly distributed and result in the incoherent addition of the resultants. In an ultrasound context, Shankar [29] showed that the Nakagami distribution could model a variety of conditions, including pre-Rayleigh, Rayleigh, and post-Rayleigh conditions and can be useful in modeling backscatter signals from the human breast [10]. The Nakagami distribution includes the Rayleigh distribution as a special case ($m = 1$) and approximates the Rician distribution for $m > 1$. Its SNR can take any positive value.

E. Weibull Distribution

The Weibull distribution was first proposed in the context of reliability engineering [30] and is described by the following pdf and cdf:

$$p(r) = \frac{b}{a}\left(\frac{r}{a}\right)^{b-1} e^{-\left(\frac{r}{a}\right)^{b}} \qquad r \geq 0;\ a, b > 0 \tag{10}$$

$$F(r) = 1 - e^{-\left(\frac{r}{a}\right)^{b}}. \tag{11}$$

In (10) and (11), b and a are the shape and scale parameters, respectively. Good evidence for this distribution has been observed in modeling radar clutter signals [31]. No theoretical explanation seems to be available for encountering this type of distribution. However, the fact that this distribution can model pre-Rayleigh, Rayleigh, and post-Raleigh conditions can be seen from the relationship between the SNR and the shape parameter b:

$$\text{SNR} = \frac{\Gamma\left(1 + \frac{1}{b}\right)}{\sqrt{\Gamma\left(1 + \frac{2}{b}\right) - \Gamma^2\left(1 + \frac{1}{b}\right)}}. \tag{12}$$

The SNR monotonically increases with b, with $0 < b < 2$ corresponding to pre-Rayleigh (SNR < 1.91), $b = 2$ corresponding to Rayleigh (SNR $= 1.91$), and $b > 2$ corresponding to post-Rayleigh or Rician (SNR > 1.91) conditions. The primary reason for including this distribution in this study is that the functional form of its pdf is different from that of the other distributions—such as the K and the Nakagami distributions—thereby increasing the search space of appropriate distributions for skin tissues. The SNR of the Weibull distribution can take any positive value.

F. Generalized Gamma Distribution

The generalized gamma distribution, hereafter referred to as the GG distribution, was introduced by Stacy [32] and is a three-parameter distribution whose pdf and cdf are given by:

$$p(r) = \frac{cr^{(cv-1)}}{a^{cv}\Gamma(v)} e^{-\left(\frac{r}{a}\right)^{c}} \qquad r \geq 0;\ a, v, c > 0 \tag{13}$$

$$F(r) = \Gamma_{\text{inc}}\left(v, \left(\frac{r}{a}\right)^{c}\right). \tag{14}$$

In (13) and (14), c and v are two-shape parameters that provide flexibility in adjusting the shape of the pdf, a is the scale parameter, and $\Gamma_{\text{inc}}(m, x)$ is the incomplete gamma function. This distribution previously was found to be useful in modeling the fading of signals in a mobile radio environment [33]. Recently, while the present work was under review, Shankar [34] independently proposed the use of this distribution to model ultrasound envelope signals. The GG distribution is especially attractive because it contains several distributions as special cases: Rayleigh ($c = 2$ and $v = 1$), exponential ($c = 1$ and $v = 1$), Nakagami ($c = 2$), Weibull ($v = 1$), and the usual gamma ($c = 1$) distribution. The lognormal distribution also arises as a limiting case when v approaches ∞. Moreover, the GG distribution provides two parameters for tissue characterization instead of, at most, one for all the other distributions. It also is interesting to note that, if r is GG distributed, so is r^2, and hence, the GG distribution can be used for modeling both the amplitude and intensity fluctuations.

For the sake of completeness, we also mention some other distributions that have been studied: the Generalized-Rician [35], [36], the Homodyned-K [37], and the Generalized-K distributions [26]. They were not used in this study because the simpler Nakagami distribution can model conditions leading to these distributions [29].

III. Methods

A. Experimental System

The experimental system and data acquisition procedure are described in detail elsewhere [20], and only brief details will be given here. The system consisted of a PVDF transducer (Panametrics, Waltham, MA, Model PI50), a pulser/receiver (Panametrics; Model PR5900), a digitizing oscilloscope sampling at 500 MHz (Tektronix, Beaverton, OR, Model TDS 520C), and a 3-axis scanning system (Parker Hannifin/Compumotor, Cleveland, OH). The characteristics of the transducer used in this study are shown in Table I. A computer was used to control both

TABLE I
CHARACTERISTICS OF THE TRANSDUCER USED IN THIS STUDY.*

Transducer	PI50 (Panametrics Inc.)
Center frequency	28 MHz
−6 dB bandwidth	30 MHz
F-number	2
Diameter	6.35 mm
Focal length	12.7 mm
−6 dB depth-of-focus	1.3 mm
Axial resolution	0.025 mm
Lateral resolution	0.1 mm

*The center frequency and −6 dB bandwidths were experimentally determined based on the spectrum of signal reflected from a perfect reflector at the transducer's focus. The F-number, diameter, and focal lengths are from the manufacturer's specifications. The depth-of-focus was experimentally determined. The axial and lateral resolutions were computed according to expressions for the −6 dB full widths.

mechanical scanning and GPIB-based data acquisition. By averaging 100 repeated acquisitions, the signal-to-noise ratio of each echo sequence was vastly improved. This approach was especially useful to record signals from subcutaneous fat, which were considerably weaker than those from the dermis. The scanning system had encoders on the x and y-axes that enabled the transducers to be positioned with an accuracy of 1 μm. Echo sequences were collected from 25 independent lateral locations of the transducers by scanning along the x and y-axes over an area of 1.5 mm × 1.5 mm in a 5 by 5 raster format. The stepping distance of 0.3 mm was larger than the lateral resolution of the system (0.1 mm). Because the transducer was well focused, diffraction effects could lead to signal variations with depth. Therefore, the transducer was axially translated to focus at a desired depth, and data were recorded from the location of the focal zone. Once the raw data were collected, further analyses were done off-line on a computer.

B. Human Subjects and Tissues

In most parts of the body, the skin consists of a thin layer of epidermis (0.15 mm thick) and a thicker underlying layer of dermis (1.2–1.8 mm thick). The region beneath the dermis consists of subcutaneous fat, which is sometimes considered as a third layer of the skin and referred to as the hypodermis. In the palms and soles, the skin is vastly different from that at other locations. Notably, the epidermal thickness is much larger (about 0.6 mm) in these regions due to the increased thickness of the stratum corneum, the dead layer of cells. In this work, data were collected from the dorsal side of forearm skin (close to the wrist) as well as the tip of the left index finger on the palmar side. Because skin conditions could depend on age, the study was restricted to only young adults. Eighteen subjects aged between 20 and 36 (median = 26) were used. In the case of the forearm region, both the dermis and subcutaneous fat tissues were studied; at the fingertip only the dermis was studied as the signals from subcutaneous fat at this region were close to the noise level. At the forearm, data collected when the focal zone was at 0.6 mm below the surface were taken to correspond to the dermis, and data collected when the focal zone was located at 2.4 mm below the surface were considered to correspond to fat. Occasionally, for some subjects, when fibrous septae were seen to be present in the fat at a depth of 2.4 mm (identified as hyperechoic structures within a relatively hypoechoic fat), another depth between 1.8 and 3.0 mm was used to extract data corresponding to fat. In the case of the fingertip, data collected when the focal zone was at 1.05 mm below the surface were taken to correspond to the dermis. For each of the experiments, a second independent repetition at a close-by region (displaced by a few millimeters from the original site) was done to increase the number of independent samples. In order to study intrasubject variability and compare it with intersubject variability, 18 repetitions of the experiment were done for one subject (male, 28 years) at the fingertip region. Water was used as a coupling medium between the transducer and the tissue. During imaging, the forearm was held steady on a table using Velcro straps. The fingertip was kept steady using custom-made finger splints.

C. Determination of Empirical Probability Density Functions

After echo sequences were recorded, the Hilbert transform approach was used to obtain envelope signals. Sixteen independent samples of the envelope signal, all lying within the focal zone region, were extracted from a particular echo sequence by picking every eighteenth sample. Assuming a speed of sound of 1.5 mm/μs in skin, the spacing between the extracted samples was 27 μm, which was larger than the axial resolution of the transducer (25 μm). Also, the total length of 405 μm spanned by all the 16 axial samples was considerably smaller than the −6 dB depth-of-focus of the transducer (1.3 mm). With 16 samples per echo sequence, 25 such echo sequences through lateral scanning (the transducer was focused at one specific depth, e.g., 0.6 mm below the surface for the case of the dermis for all the 25 echo sequences), and two repetitions of the experiment, a total of 800 samples were available to construct empirical histograms. Before combining the samples in the above manner, compensation for attenuation within the 405 μm distance was done by assuming attenuation coefficient slopes of 0.21, 0.18, and 0.33 dB/mm/MHz for the forearm dermis, forearm fat, and fingertip dermis, respectively [20]. Also, occasional specular reflectors (e.g., fibrous septae in subcutaneous fat) were eliminated prior to analysis to the extent possible. Such occasional specular reflectors would make the results more pre-Rayleigh than the ones reported in this work [36] and were removed because they were considered extraneous to the tissue of interest.

D. Estimation of the Parameters

Estimation of the parameters of all six distributions was done using the maximum likelihood (ML) method,

in which the set of parameters that maximizes the likelihood function or its logarithm is determined. In the case of the Rayleigh distribution, the ML parameter was obtained using a closed-form expression:

$$\hat{\sigma}^2_{ML} = \frac{E(r^2)}{2}. \tag{15}$$

In this paper, $E(x)$ represents the mean of the random variable x, and is taken to be equal to the sample mean. For distributions other than Rayleigh, simple closed-form solutions for the parameters do not exist, and the ML procedure was implemented as an optimization problem that sought to determine parameters which maximized the log-likelihood function. The optimization procedure was implemented using the Nelder-Mead Simplex method [38] available in the Matlab optimization toolbox (The Math Works Inc., Natick, MA). This method does not require the computation of derivatives but requires an initial guess of the solution. The initial guesses of the parameters (denoted with subscript 0 in this paper) were obtained using the method of moments as described below. For the Rician, K, and Nakagami distributions, the initial guesses were obtained using estimated second and fourth moments of the data. For the Rician distribution we have:

$$s_0 = \sqrt[4]{2\left[E\left(r^2\right)\right]^2 - E\left(r^4\right)} \tag{16}$$

$$\sigma_0 = \sqrt{\frac{E\left(r^2\right) - s_0^2}{2}}. \tag{17}$$

For the K distribution we have:

$$\alpha_0 = \frac{2}{\dfrac{E\left(r^4\right)}{\left[E\left(r^2\right)\right]^2} - 2} \tag{18}$$

$$b_0 = \sqrt{\frac{4\alpha_0}{E\left(r^2\right)}}. \tag{19}$$

For the Nakagami distribution the initial guesses were obtained as:

$$m_0 = \frac{\left[E\left(r^2\right)\right]^2}{E\left(r^4\right) - \left[E\left(r^2\right)\right]^2} \tag{20}$$

$$\Omega_0 = E\left(r^2\right). \tag{21}$$

Under some conditions, (16)–(19) for the Rician and K distributions do not yield meaningful solutions. For instance, if the data were truly pre-Rayleigh distributed (e.g., K distributed), the computed value of s_0 would be complex. This was indeed the case for almost all of the data obtained (see Section IV). The ML procedure for the Rician distribution was implemented by assuming the initial guess s_0 to be a small positive quantity, equal to 0.1. However, if the data were truly Rician distributed, the computed value of α_0 would be negative. But no such problem was seen for all the data sets analyzed in this paper.

For the Weibull distribution, an iterative procedure was used to compute the initial guess b_0 by solving the following equation:

$$\frac{\Gamma\left(1+\dfrac{2}{b_0}\right)}{\Gamma^2\left(1+\dfrac{1}{b_0}\right)} = \frac{E\left(r^2\right)}{\left[E(r)\right]^2}. \tag{22}$$

It can be shown that the LHS of (22) is a monotonic function of b_0; therefore, a unique solution exists. The solution was obtained using a look-up table containing precomputed values of the LHS as a function of finely spaced b_0 (accuracy of estimate was 0.005 in the range $1 \leq b_0 \leq 2$, where the solution was found for the data sets in this work). Once b_0 was obtained, a_0 was obtained from the following expression:

$$a_0 = \frac{E(r)}{\Gamma\left[1+\dfrac{1}{b_0}\right]}. \tag{23}$$

For the GG distribution, the initial guesses for the parameters were obtained using the moments of logarithm of data as proposed by Stacy and Mihram [39]:

$$\frac{\psi''(v_0)}{\left[\psi'(v_0)\right]^{1.5}} = -\left|\frac{E\left[\left(\ln(r) - \overline{\ln(r)}\right)^3\right]}{\left\{E\left[\left(\ln(r) - \overline{\ln(r)}\right)^2\right]\right\}^{1.5}}\right| \tag{24}$$

$$c_0 = \sqrt{\frac{\psi'(v_0)}{E\left[\left(\ln(r) - \overline{\ln(r)}\right)^2\right]}} \tag{25}$$

$$a_0 = E(r)\frac{\Gamma(v_0)}{\Gamma\left(v_0 + \dfrac{1}{c_0}\right)}. \tag{26}$$

In (24) and (25), $\psi^n(v) = \dfrac{d^{n+1}}{dv^{n+1}}\ln[\Gamma(v)]$ is the polygamma function, which was evaluated using the polygamma function in Matlab's Symbolic Toolbox. At first, v_0 was obtained by solving (24), where the RHS of this equation is the skewness of the logarithm of the data. Fig. 1 shows a plot of the LHS of (24) as a function of v_0. It can be seen that this function is monotonic; hence, a unique solution for v_0 exists as long as the RHS is between -2 and 0, which was the case for all the data sets analyzed in this work. A look-up table with precomputed values of the LHS as a function of v_0 was used for this purpose (accuracy of estimate was 0.005 for the values estimated in this work). After v_0 was obtained, the value of c_0 was obtained using (25), and subsequently the value of a_0 was obtained using (26).

After the initial guesses of the parameters of the Rician, K, Nakagami, Weibull, and the Generalized Gamma distributions were obtained as described above, the ML estimation was implemented using the Nelder-Mead optimization technique. We note that there are other simpler

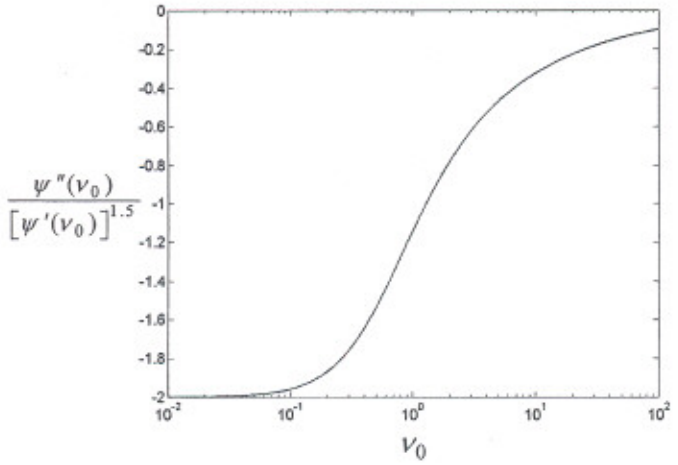

Fig. 1. Computation of the initial guess of the GG-υ parameter. The graph shows the LHS of (24) as a function of the parameter ν_0.

methods to compute the parameters of some of the above distributions [40], including the use of fractional order moments [41]. However, in order to compare the capability of various distributions to model data from tissues, it is preferable to use the same method for estimating the parameters of all the distributions. Thus, the ML method was used for estimating the parameters of all the distributions. Also, the Nelder-Mead technique provided a uniform scheme to implement the ML method for the various distributions, although we note that alternate implementations of the ML method also are possible [42].

E. Numerical Issues

One issue in implementing the ML estimation procedure is that proper care is needed to prevent overflow problems while computing the log-likelihood functions. For example, the gamma function present in expressions for the pdfs of some of the distributions could easily overflow the maximum limit of most computers when its argument is large. However, its logarithm has a much smaller value; therefore, while computing the log-likelihood functions, a direct evaluation of the logarithm of the gamma function was used. Also, while computing the log-likelihood functions for the K distribution, the Bessel function $K_{\alpha-1}(x)$ could overflow the maximum limit of computers for small values of x. Hence, an exponential approximation was used in such cases [43]:

$$K_{\alpha-1}(x) \simeq \frac{\Gamma(\alpha-1)}{2}\left(\frac{2}{x}\right)^{\alpha-1} \quad \text{for } x \ll \alpha - 1. \tag{27}$$

The logarithm of the above function was evaluated directly without first computing the exponential, thereby avoiding numerical overflows.

F. Goodness of Fit Testing

The goodness of fit of each of the candidate distributions to the empirical distribution was evaluated using the KS goodness of fit measure, which is the maximum absolute difference between the fitted cdf and the empirical cdf [44]. A smaller value of the KS statistic indicates a better fit of the particular distribution to empirical data. For computing the fitted cdfs, the expressions given in Section II were used. The KS test also enables us to accept or reject the hypothesis that a particular distribution could model the empirical data for a chosen level of significance. For example, for a significance level of 0.01, in order to accept the model, the KS value should be less than (see Table A14 in [44]):

$$D = \frac{1.63}{\sqrt{N}}, \tag{28}$$

which for a sample size of $N = 800$ is 0.0576.

G. Statistical Tests

To study the capability of the parameters of the various distributions to differentiate different tissue types (dermis vs. fat; forearm dermis vs. fingertip dermis), the Wilcoxon sign rank test (without the normal approximation for the test statistic) was used. In this test, the two values being compared are taken as paired samples.

IV. Results

A. Probability Density Function of Amplitude of Backscattered Signals from Skin Tissues

Fig. 2 shows typical pdf fits to empirical envelope data obtained at the forearm of a human subject in vivo for all the six distributions. The fits were obtained using the ML method for estimating the parameters with a sample size of 800. It can be seen that the GG pdf fitted the empirical histograms very well and had the smallest KS value compared to the other distributions. The empirical histograms were pre-Rayleigh, and the Rayleigh and Rician distributions modeled the empirical histograms poorly compared to the other distributions. Also, the best Rayleigh and Rician fits were almost the same, which is consistent with the fact that the best Rician fit to data that are pre-Rayleigh distributed is the Rayleigh fit. Other distributions, especially the K and Weibull distributions, also show good fits to the data. The empirical histogram for the case of fat was more pre-Rayleigh than that of the dermis.

Fig. 3 shows the KS goodness of fit measures between each one of the six distributions and the empirical distribution for the forearm dermis, forearm fat, and fingertip dermis. The GG distribution provided the best fit in a majority of cases, and on the average had the smallest KS statistic values. Next to the GG distribution, the K and Weibull distributions also provided good fits to the data as seen by the closeness of their KS values to that of the GG distribution. If a hypothesis test was undertaken at a significance level of 0.01 to accept or reject each of the models, the KS values should be less than $1.63/\sqrt{N}$, which for $N = 800$ is 0.0576. It can be seen from Fig. 3 that, on the

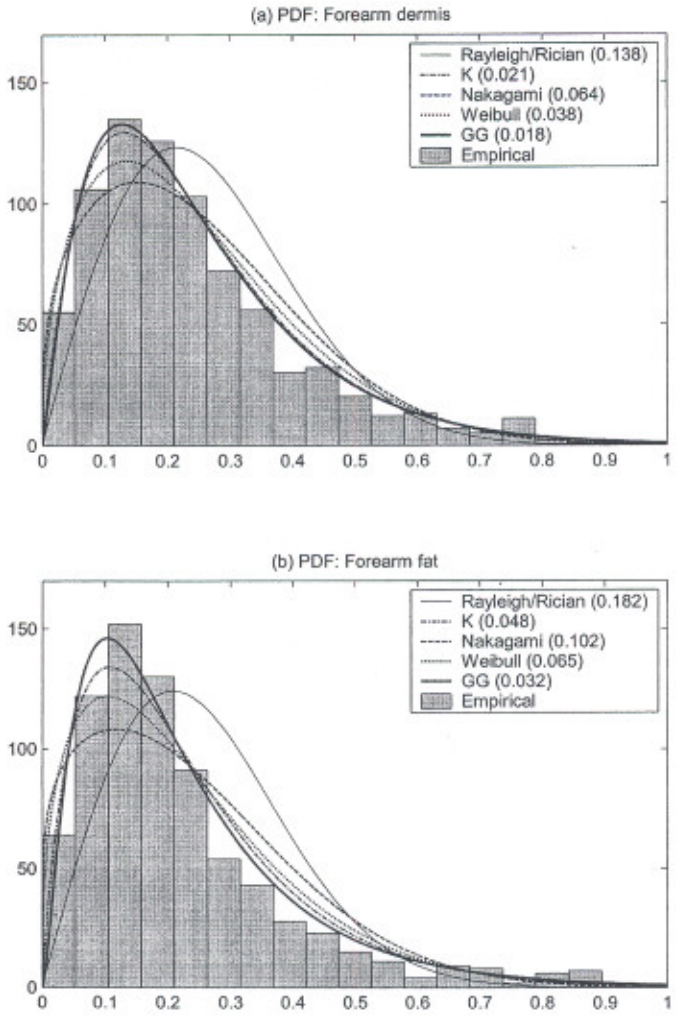

Fig. 2. Fitting probability density functions to empirical data. (a) Corresponds to data from the forearm dermis; (b) corresponds to data from the forearm fat. The pdf fits were scaled so that the area under the curves matched the total area under the histograms. The samples were normalized so that the maximum value was unity. The Rayleigh and Rician fits are colinear. The values in the inset are the KS goodness of fit values.

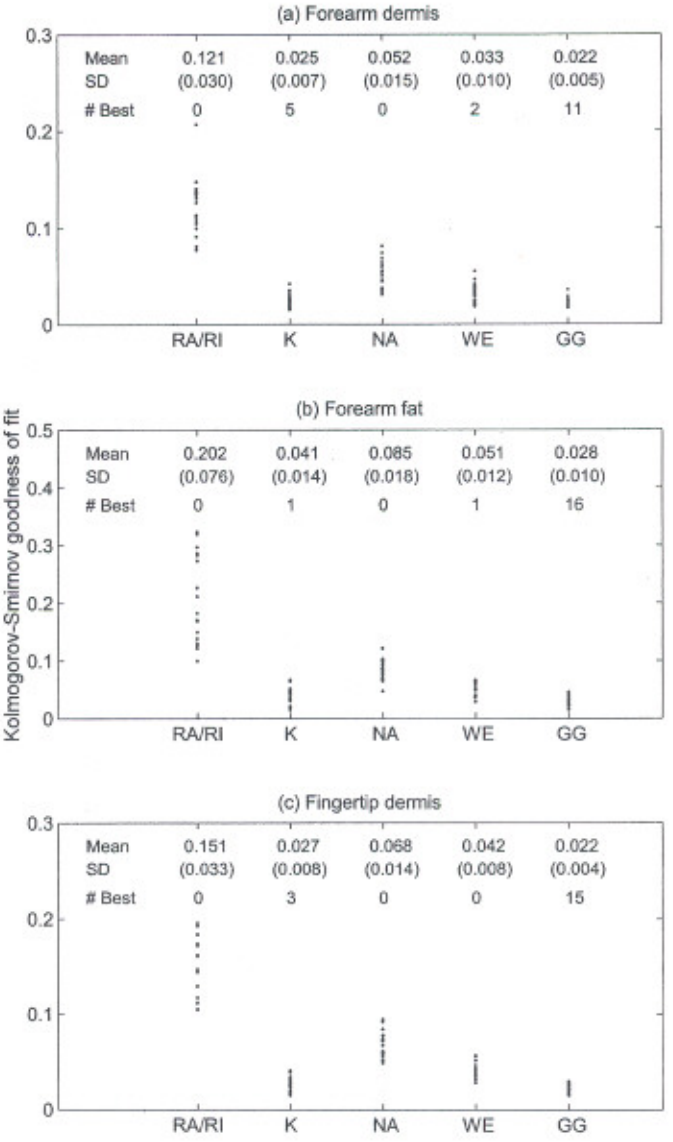

Fig. 3. The KS goodness of fit measure between the empirical distribution and each of the six fitted distributions (RA-Rayleigh, RI-Rician, K-K, NA-Nakagami, WE-Weibull, GG-Generalized Gamma) for the (a) dermis and (b) fat at the forearm wrist and the (c) dermis at the fingertip. Each dot corresponds to data from one particular subject. The mean, standard deviation (SD), and the number of subjects for which the KS value of that particular distribution was the best (smallest), are indicated.

average, the GG, K, and Weibull distributions would satisfy this criterion for all three tissues. The Nakagami distribution, although better than the Rayleigh/Rician models, did not fit the data as well as the GG, K, and Weibull distributions. For all the data sets, the Rayleigh and Rician distributions gave poor fits to the data, and hence their parameters were not studied further.

B. Intersubject Variability vs. Intrasubject Variability

Fig. 4 shows a plot of the estimates of the SNR parameter and of the shape parameters of the K, Nakagami, Weibull, and GG distributions for all the subjects, and for 18 repetitions on the same subject. All the data were obtained at the fingertip. For both the inter- and intrasubject cases, the SNR and Weibull-b parameters showed smaller variability (5–7% of the mean) than the other parameters. The K and GG distribution parameters showed larger variability (17–43% of the mean). The Nakagami-m parameter showed about 9% variability with respect to the mean. For the SNR, Nakagami-m, and Weibull-b parameters, the percent variability was only marginally smaller for the intersubject case than for the intrasubject case. Given that these parameters are positively biased, the smaller variability in the intrasubject case could be accounted for by the smaller mean values. In the case of the K-α and GG-c parameters, the percent variability was smaller for the intrasubject case, but once again these could be explained by the differences in mean values. For the GG-v parameter, the intersubject variability was larger even though the means were comparable, but it is conceivable that the vari-

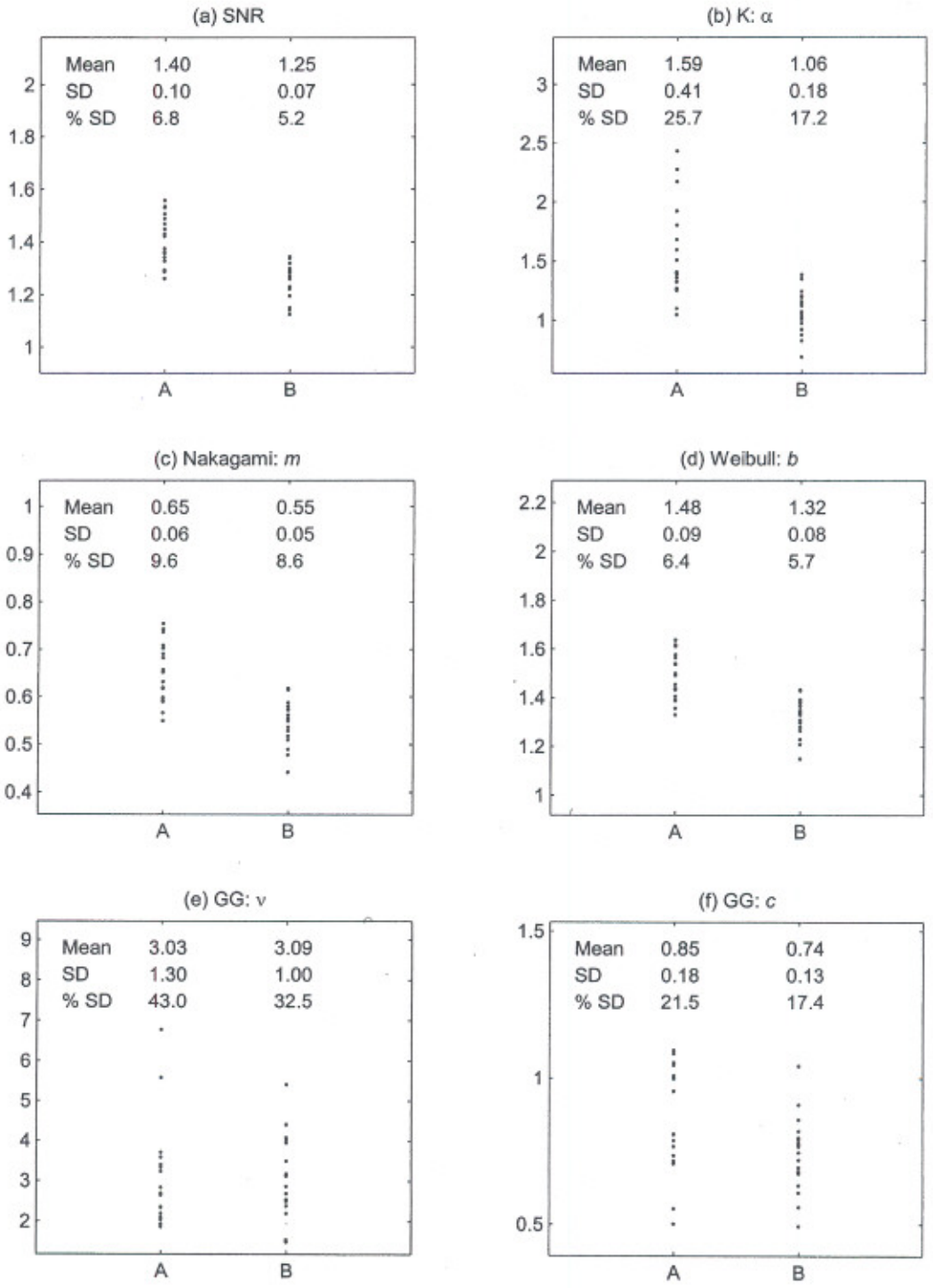

Fig. 4. Comparison between intersubject (A) and intrasubject (B) variability. The dots represent the estimated values for each subject or repetition. Numerical values for the mean (top row), the standard deviation (middle row), and the percentage variability defined as $\frac{\text{mean}}{\text{SD}} \times 100$ (bottom row) also are indicated.

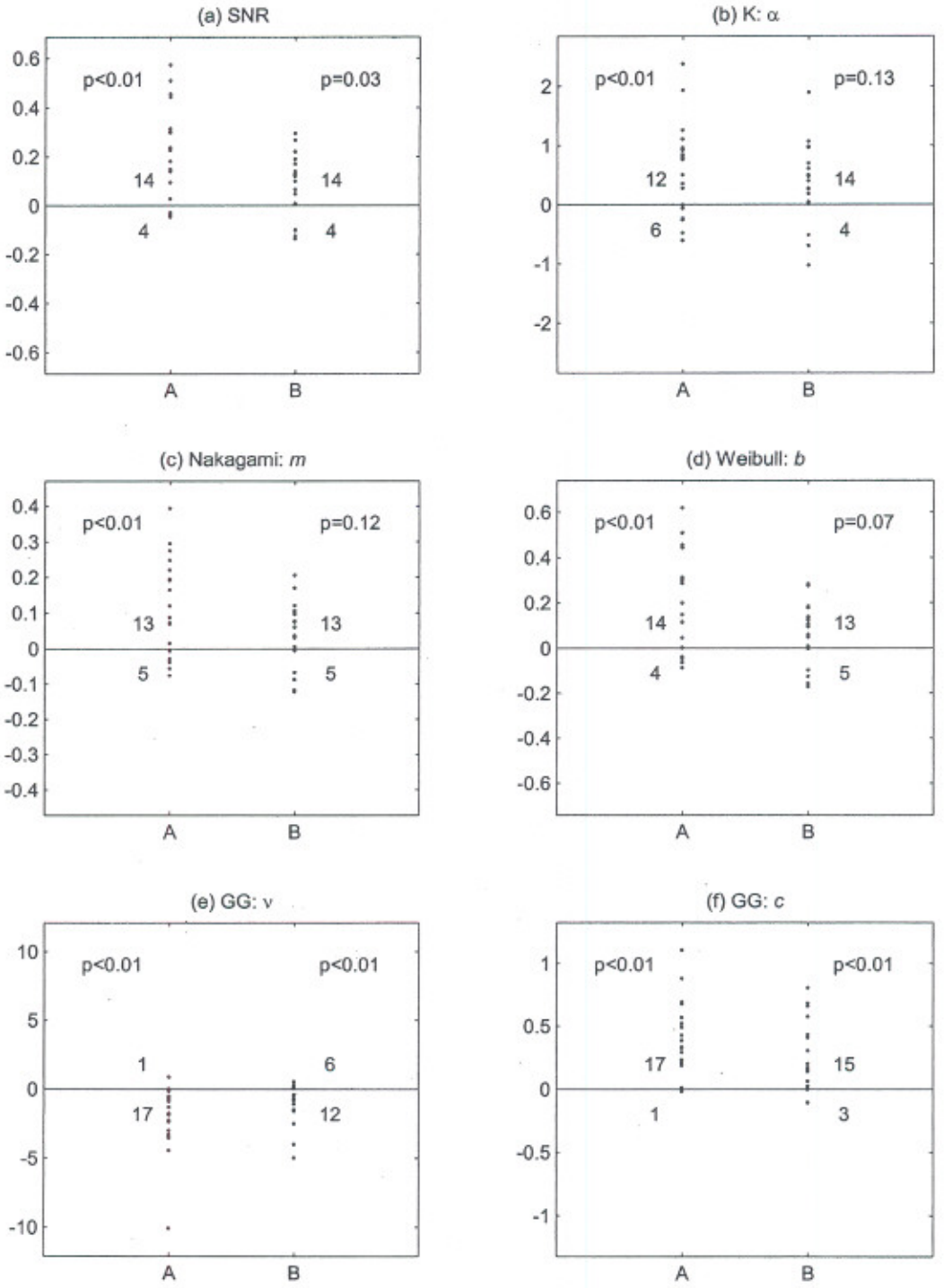

Fig. 5. Differences in parameters between the dermis and fat at the forearm (A) and the dermis at the forearm and fingertip (B). Each data point is the difference in the respective estimated quantities. The number above and below the $y = 0$ line indicate the number of cases in which the difference values were positive and negative, respectively. The p-values based on a Wilcoxon sign rank test also are indicated.

ability could have been lower than the intrasubject case if a couple of extreme values had been excluded [Fig. 4(e)]. These results suggest that the inter- and intrasubject variability in the parameter estimates are similar. Although the particular subject chosen for the intrasubject may not be characteristic of all subjects, the similarity in intra- and intersubject variability indicates that reasons other than genuine intersubject differences might be important and suggests further work for identifying and reducing variability.

C. Characterization of Differences in Tissues

The SNR parameter and the shape parameters of the K, Nakagami, Weibull, and GG distributions were evaluated for their capability to differentiate between the dermis and fat at the forearm, and between the dermis at the forearm and fingertip regions. For this purpose, the difference in the estimated parameters between the two tissues taken subjectwise were computed. The data to compare forearm dermis and fat were obtained from the same experiment in which the location of the transducer focal zone was axially shifted to focus first on the dermis and subsequently on fat. The data to compare the forearm and fingertip dermis were obtained from two separate experiments done one after the other at the two body sites. From Fig. 5 it can be seen that the differences in parameter estimates between the dermis and fat was positive in a majority of the cases for SNR, K-α, Nakagami-m, Weibull-b, and GG-c parameters, and negative in a majority of cases for the GG-v parameter. For all parameters, significant differences between the dermis and fat could be seen as indicated by low p-values. Between forearm dermis and fingertip dermis, a similar trend is seen, but only the GG parameters showed significant differences at a 0.01 significance level. These results indicate that the GG-v and GG-c parameters might be more capable of differentiating tissues than the other parameters.

V. Discussion

Skin is an easily accessible organ in the human body and is affected by a large number of lesions. With conventional ultrasound, it is often difficult to distinguish between various lesions and, hence, additional quantitative studies might be useful. One such method is the use of envelope statistics. This study seems to be the first one on modeling the pdf of envelope signals from skin tissues. The statistics of envelope signals can provide additional information only if the statistics deviate from the Rayleigh behavior. If only Rayleigh statistics were present, no additional information other than the mean backscatter level can be used for tissue characterization. This study supports the hypothesis that non-Rayleigh, specifically pre-Rayleigh statistics, are present in the case of skin tissues (at least for the specific transducer used), which, therefore, can provide additional information for tissue characterization. However, the non-Rayleigh behavior cannot automatically be ascribed to the small resolution cell sizes present in high-frequency imaging systems. This is because tissues contain scatterers even at small length scales, and the number of scatterers is not necessarily small for small resolution cell sizes. For example, collagen fibers, the dominant scatterers in the dermis, are themselves composed of smaller fibrils and microfibrils, all of which constitute scatterers ranging in size from tens of microns to tens of Angstroms [45], [46]. It is likely that the variation in scatterer cross sections is large enough to cause the effective number of scatterers within the resolution cell to be small, leading to pre-Rayleigh statistics. It also should be pointed out that the envelope statistics are not only dependent on the tissue being studied, but also are dependent on the imaging system used. When a less focused transducer (f/#=4, but similar frequency characteristics to the one reported in this work) was used, the mean estimated SNR values were about 9% larger for both the dermis and fat tissues (results based on this transducer are not reported in this work). This is consistent with the fact that the resolution cell size is larger for a less focused transducer than a more focused transducer, leading to less pre-Rayleigh deviations.

Previous studies (involving other tissues) have rarely compared the performance of several distributions for modeling empirical data. Also, except for the recently published independent work by Shankar [34], the applicability of the GG distribution has not been studied in an ultrasound context. Our study shows that the GG distribution was able to fit the empirical envelope data from skin tissues better than all the other distributions. This is not surprising as the GG distribution has one additional parameter that makes it more flexible to tailor itself to empirical data as long as a sufficient sample size is available. However, it should be noted that, even among distributions with the same number of parameters, some of them fit better than the others. For example, the K and Weibull distributions fit better than the Rician and Nakagami distributions even though all of them have two parameters, implying that the number of parameters does not solely determine the goodness of fit. Thus, the better fit of the GG distribution is not merely because of having an additional parameter, but rather because of its ability to adjust its upper and lower tails independently with two-shape parameters [33], [34]. Other distributions, especially the K and Weibull distributions, also were able to model the envelope data well. In practice, the choice of an appropriate distribution will depend not only on the goodness of fit, but also on other factors, including the variability in the estimated parameters, the sample size available (which is related to the variability), and the capability of the estimated parameters to classify different tissues. Even though all the parameters were estimated using the same sample size, the GG-v parameter showed larger percent variations than the other parameters. This would imply that, in general, a larger sample size would be necessary to estimate the GG parameters to a desired level of accuracy. Such variability issues regarding the GG distribution have been studied before, because of which the Weibull distribution has of-

ten been considered appropriate when the sample size is small [47]. The K distribution yielded very good goodness of fit measures, but it showed more variability than the Weibull parameters. It is known that the K distribution becomes less useful when the true value of α is large, because the variance in the estimate becomes large [12]. The Weibull and Nakagami distributions do not have this difficulty. Between the Weibull and Nakagami distributions, the Weibull distribution outperformed the Nakagami distribution with better goodness of fits as well as a smaller percent variability. It is likely that the Weibull and GG distributions might prove useful in modeling ultrasound echo signals when small and large sample sizes are available, respectively.

One would expect the intrasubject variability in the parameters to be smaller than the intersubject variability as additional differences from one subject to another could arise due to different skin conditioning, aging, or sun exposure. However, the intrasubject variability was found to be similar to intersubject variability for data collected at the fingertip. This indicates that any genuine variability between subjects is overshadowed by other factors. One possible reason is the finite sample size used to estimate the parameters. Increasing the sample size could reduce variability but only at the loss of stationarity in tissue properties. Other possible factors include variations in ambient humidity, time to acclimatize to the ambient conditions, and diurnal changes associated with skin [48]. The fact that intrasubject variability is large indicates that, for tissue characterization, data should preferably be acquired from both the suspected lesion and the adjoining normal skin tissue during the same experiment itself.

Dermis and fat are vastly different tissues. They easily can be differentiated using the absolute backscatter levels in the frequency range 20–50 MHz [20]. The present work supports the hypothesis that they can be differentiated using envelope statistics as well. This was despite the variability in the estimated parameters. Fat was seen to show more pre-Rayleigh behavior as shown by smaller SNR values. More deviation from Rayleigh to pre-Rayleigh is the result of more variations in the scattering cross sections, or equivalently, smaller effective number of scatterers in fat. Such variations in fat tissue could be due to the presence of septa/fascia, adding to the inhomogeneity of the tissue. Between the dermis at the fingertip and forearm regions, only the GG parameters showed differences at a 0.01 significance level, indicating that the GG distribution might be better suited in classifying skin tissues than other distributions (if a sufficient sample size is available). While computing the parameter estimates for the case of forearm fat, the effect of intervening attenuation (not the same as attenuation within the region of interest) by the dermis, and to a lesser extent the much thinner epidermis, was not considered. The presence of intervening attenuation would tend to increase the size of the resolution cell, thereby pushing the distributions closer to the Rayleigh distribution [49]. This would lead to larger estimates for parameters such as K-α, Nakagami-m, and Weibull-b. However, even in the presence of intervening attenuation, the above parameters were found to be smaller for fat than for the dermis. Intervening attenuation also will affect the parameters estimated at the fingertip dermis due to the thicker epidermis. Hence, it is conceivable that the true estimates of the above parameters for the forearm fat and fingertip dermis are smaller than what was estimated. Such effects can be minimized using narrow-band filtering prior to estimation. In future work we plan to study the capability of the parameters of non-Rayleigh distributions to differentiate specific skin lesions from normal skin tissues.

References

[1] B. D. Fornage, M. H. McGavran, M. Duvic, and C. A. Waldron, "Imaging of the skin with 20-MHz US," *Radiology*, vol. 189, pp. 69–76, 1993.

[2] T. Cammarota, F. Pinto, A. Magliaro, and A. Sarno, "Current uses of diagnostic high-frequency US in dermatology," *Eur. J. Radiol.*, vol. 27, pp. 215–223, 1998.

[3] D. H. Turnbull, B. G. Starkoski, K. A. Harasiewicz, J. L. Semple, L. From, A. K. Gupta, D. N. Sauder, and F. S. Foster, "A 40-100 B-scan ultrasound backscatter microscope for skin imaging," *Ultrasound Med. Biol.*, vol. 21, pp. 79–88, 1995.

[4] K. Hoffmann, J. Jung, S. El Gammal, and P. Altmeyer, "Malignant melanoma in 20 MHz B scan sonography," *Dermatology*, vol. 185, pp. 49–55, 1992.

[5] G. Sommer, R. Stern, and H. Chen, "Cirrhosis: US images with narrow band filtering," *Radiolology*, vol. 165, pp. 425–430, 1987.

[6] B. J. Oosterveld, J. M. Thijssen, P. C. Hartman, and G. J. E. Rosenbusch, "Detection of diffuse liver disease by quantitative echography: Dependence on *a priori* choice of parameters," *Ultrasound Med. Biol.*, vol. 19, pp. 21–25, 1993.

[7] I. Schnittger, A. Vieli, J. E. Heiserman, B. A. Director, M. E. Billingham, S. G. Ellis, R. S. Kernoff, T. Takamoto, and R. L. Popp, "Ultrasonic tissue characterization: Detection of acute myocardial ischemia in dogs," *Circulation*, vol. 72, pp. 193–199, 1985.

[8] K. A. Wear, T. A. Shoup, and R. L. Popp, "Ultrasonic characterization of canine myocardium contraction," *IEEE Trans. Ultrason., Ferroelect., Freq. Contr.*, vol. UFFC-33, pp. 347–353, 1986.

[9] L. Clifford, P. Fitzgerald, and D. James, "Non-Rayleigh first-order statistics of ultrasonic backscatter from normal myocardium," *Ultrasound Med. Biol.*, vol. 19, pp. 487–495, 1993.

[10] P. M. Shankar, V. A. Dumane, J. M. Reid, V. Genis, F. Forsberg, C. W. Piccoli, and B. B. Goldberg, "Classification of ultrasonic B-mode images of breast masses using Nakagami distribution," *IEEE Trans. Ultrason., Ferroelect., Freq. Contr.*, vol. 48, pp. 569–580, 2001.

[11] R. L. Romijn, J. M. Thijssen, B. J. Oosterveld, and A. M. Verbeek, "Ultrasonic differentiation of intraocular melanomas: Parameters and estimation methods," *Ultrason. Imaging*, vol. 13, pp. 27–55, 1991.

[12] K. A. Wear, R. F. Wagner, D. G. Brown, and M. F. Insana, "Statistical properties of estimates of signal-to-noise ratio and number of scatterers per resolution cell," *J. Acoust. Soc. Amer.*, vol. 102, pp. 635–641, 1997.

[13] G. E. Sleefe and P. P. Lele, "Tissue characterization based on scatterer number density estimation," *IEEE Trans. Ultrason., Ferroelect., Freq. Contr.*, vol. 35, pp. 749–757, 1988.

[14] J.-F. Chen, E. L. Madsen, and J. A. Zagzebski, "A method for determination of frequency-dependent effective scatterer number density," *J. Acoust. Soc. Amer.*, vol. 95, pp. 77–85, 1994.

[15] R. F. Wagner, M. F. Insana, and D. G. Brown, "Statistical properties of radio-frequency and envelope-detected signals with applications to medical ultrasound," *J. Acoust. Soc. Amer.*, vol. 4, pp. 910–922, 1987.

[16] C. M. Moran, N. L. Bush, and J. C. Bamber, "Ultrasonic propagation properties of excised human skin," *Ultrasound Med. Biol.*, vol. 21, pp. 1177–1190, 1995.

[17] T. Baldeweck, P. Laugier, and G. Berger, "An in vitro study on porcine skin: Attenuation profile estimation using auto-

regressive modeling," in *Proc. IEEE Ultrason. Symp.*, vol. 2, pp. 1141–1144, 1995.
[18] L. Pan, L. Zan, and F. S. Foster, "Ultrasonic and viscoelastic properties of skin under transverse mechanical stress *in vitro*," *Ultrasound Med. Biol.*, vol. 24, pp. 995–1007, 1998.
[19] C. Guittet, F. Ossant, L. Vaillant, and M. Berson, "In vivo high frequency ultrasonic characterization of human dermis," *IEEE Trans. Biomed. Eng.*, vol. 46, pp. 740–746, 1999.
[20] B. I. Raju and M. A. Srinivasan, "High-frequency ultrasonic attenuation and backscatter coefficients of in vivo normal human dermis and subcutaneous fat," *Ultrasound Med. Biol.*, vol. 27, pp. 1543–1556, 2001.
[21] J. S. Daba and M. R. Bell, "Statistics of the scattering cross-section of a small number of random scatterers," *IEEE Trans. Antennas Propagat.*, vol. 43, pp. 773–783, 1995.
[22] J. W. Strutt (Lord Rayleigh), "On the resultant of a large number of vibrations of the same pitch and of arbitrary phase," *Philosophical Magazine (Series 5)*, vol. 10, pp. 73–78, 1880.
[23] S. O. Rice, "Statistical properties of a sine wave plus random noise," *Bell. Syst. Tech. J.*, vol. 27, pp. 109–157, 1948.
[24] J. G. Proakis, *Digital Communications*. New York: McGraw-Hill, 2000.
[25] E. Jakeman and P. N. Pusey, "A model for non-Rayleigh sea echo," *IEEE Trans. Antennas Propagat.*, vol. AP-24, pp. 806–814, 1976.
[26] E. Jakeman and R. J. A. Tough, "Generalized K distribution: A statistical model for weak scattering," *J. Opt. Soc. Amer.*, vol. 4, pp. 1764–1772, 1987.
[27] M. Nakagami, "The m-distribution—A general formula of intensity distribution of rapid fading," in *Statistical Methods in Radio Wave Propagation*. W. C. Hoffman, Ed. New York: Pergamon, 1960, pp. 3–36.
[28] M. D. Yacoub, "Fading distributions and co-channel interference in wireless systems," *IEEE Antennas Propagat. Mag.*, vol. 42, pp. 150–158, 2000.
[29] P. M. Shankar, "A general statistical model for ultrasonic backscattering from tissues," *IEEE Trans. Ultrason., Ferroelect., Freq. Contr.*, vol. 47, pp. 727–736, 2000.
[30] W. Weibull, "A statistical distribution function of wide applicability," *J. Appl. Mech.*, vol. 18, pp. 293–297, 1951.
[31] D. Fernandes and M. Sekine, "Suppression of Weibull radar clutter," *IEICE Trans. Comm.*, vol. E76-B, pp. 1231–1235, 1993.
[32] E. W. Stacy, "A generalization of the gamma distribution," *Annal. Math. Stat.*, vol. 33, pp. 1187–1192, 1962.
[33] A. J. Coulson, A. G. Williamson, and R. G. Vaughan, "Improved fading distribution for mobile radio," *IEEE Proc. Commun.*, vol. 145, pp. 197–202, 1998.
[34] P. M. Shankar, "Ultrasonic tissue characterization using a generalized Nakagami model," *IEEE Trans. Ultrason., Ferroelect., Freq. Contr.*, vol. 48, pp. 1716–1720, 2001.
[35] M. F. Insana, R. F. Wagner, B. S. Gara, D. G. Brown, and T. H. Shawker, "Analysis of ultrasound image texture via generalized Rician statistics," *Opt. Eng.*, vol. 25, pp. 743–748, 1986.
[36] T. A. Tuthill, R. H. Sperry, and K. J. Parkar, "Deviations from Rayleigh statistics in ultrasonic speckle," *Ultrason. Imaging*, vol. 10, pp. 81–89, 1988.
[37] V. Dutt and J. Greenleaf, "Ultrasound echo envelope analysis using a homodyned K distribution signal model," *Ultrason. Imaging*, vol. 16, pp. 265–287, 1994.
[38] J. A. Nelder and R. Mead, "A simplex method for function minimization," *Comput. J.*, vol. 7, pp. 308–313, 1965.
[39] E. W. Stacy and G. A. Mihram, "Parameter estimation for a generalized gamma distribution," *Technometrics*, vol. 7, pp. 349–358, 1965.
[40] R. S. Raghavan, "A method for estimating parameters of K-distributed clutter," *IEEE Trans. Aerosp. Electron. Syst.*, vol. 27, pp. 238–246, 1991.
[41] V. Dutt and J. Greenleaf, "Speckle analysis using signal to noise ratios based on fractional order moments," *Ultrason. Imaging*, vol. 17, pp. 251–268, 1995.
[42] D. R. Wingo, "Computing maximum-likelihood parameter estimates of the generalized gamma distribution by numerical root isolation," *IEEE Trans. Rel.*, vol. 36, pp. 586–590, 1987.
[43] M. Abramowitz and I. A. Stegun, *Handbook of Mathematical Functions*. New York: Dover, 1965.
[44] W. J. Conover, *Practical Nonparametric Statistics*. New York: Wiley, 1980.
[45] I. Brown, "Scanning electron microscopy of human dense fibrous tissue," *J. Anat.*, vol. 113, pp. 159–168, 1972.
[46] W. Montagna and P. F. Parakkal, *The Structure and Function of Skin*. New York: Academic, 1974.
[47] H. W. Hager and L. J. Bain, "Inferential procedures for the generalized gamma distribution," *J. Amer. Statist. Assoc.*, vol. 65, pp. 1601–1609, 1970.
[48] M. Gniadecka, R. Gniadecki, J. Serup, and J. Sondergaard, "Ultrasound structure and digital image analysis of the subepidermal low echogenic band in aged human skin: Diurnal changes and interindividual variability," *J. Invest. Dermatol.*, vol. 102, pp. 362–365, 1994.
[49] J. A. Zagzebski, J.-F. Chen, F. Dong, and T. Wilson, "Intervening attenuation affects first-order statistical properties of ultrasound echo signals," *IEEE Trans. Ultrason., Ferroelect., Freq. Contr.*, vol. 46, pp. 35–40, 1999.

Balasundar I. Raju was born in Madras, India, in 1972. He received the bachelor's degree in mechanical engineering from the Indian Institute of Technology, Madras, in 1994. He received two master's degrees, one in mechanical engineering and one in electrical engineering and computer science, both from MIT in 1998. He is currently a Ph.D. candidate in the Department of Electrical Engineering and Computer Science at MIT.

He has spent two summers in the industry working on linear and nonlinear ultrasonic wave propagation problems. His research interests include high-frequency ultrasound, wave propagation, signal and image processing, skin imaging and characterization, and skin biomechanics.

Mandayam Srinivasan received the bachelor's degree in civil engineering from Bangalore University, India, the master's degree in aeronautical engineering from the Indian Institute of Science, Bangalore, India, and the Ph.D. degree in applied mechanics from Yale University, Princeton, NJ. He worked as a member of the research staff at the Department of Anesthesiology, Yale University School of Medicine, where he conducted research on the mechanics and mechanisms of the primate sense of touch. Since 1987 he has been at the Massachusetts Institute of Technology (MIT), Cambridge, where he founded the Laboratory for Human and Machine Haptics, informally known as the Touch Lab (http://touchlab.mit.edu). He is currently the Director of the Touch Lab and a principal research scientist with the Department of Mechanical Engineering and the Research Laboratory of Electronics at MIT.

Dr. Srinivasan has conducted pioneering investigations in skin biomechanics, tactile neuroscience, sensorimotor psychophysics, haptic device design, and multimodal rendering algorithms. He has demonstrated novel applications of this multidisciplinary research in areas such as the development of multiuser haptics in shared virtual environments, medical simulations involving force feedback for training, and direct control of machines from primate brain signals. As part of the research on human haptics, he has worked on a variety of techniques for imaging the skin, including video-microscopy, MRI, optical coherence tomography (OCT), and high frequency ultrasound.

Dr. Srinivasan has served as a member of the National Academy of Sciences committee on virtual reality and teleoperator systems, the MIT Virtual Environment and Teleoperation Research Consortium, and the editorial board of the MIT Press journal, *Presence: Teleoperators and Virtual Environments*. Dr. Srinivasan is also a member of the Society for Neuroscience. His work has been featured in print, radio, and television media around the world in news articles and programs focused on cutting-edge research in information technology and its future prospects.